1-1-2015

An assessment of image distortion and CT number accuracy within a wide-bore CT extended field of view

Bradley Beeksma
Ingham Institute, Liverpool, bb401@uowmail.edu.au

D Truant
Ingham Institute, Liverpool

Lois C. Holloway
University of Wollongong, loish@uow.edu.au

Sankar Arumugam
Ingham Institute, Liverpool

An assessment of image distortion and CT number accuracy within a wide-bore CT extended field of view

Abstract

Although wide bore computed tomography (CT) scanners provide increased space for patients, the scan field of view (sFOV) remains considerably smaller than the bore size. Consequently, patient anatomy which spans beyond the sFOV is truncated and the information is lost. As a solution, some manufacturers provide the capacity to reconstruct CT images from a partial dataset at an extended field of view (eFOV).

To assess spatial distortion within this eFOV three phantoms were considered a 30 x 30 x 20 cm^3 slab of solid water, the Gammex electron density CT phantom and a female anthropomorphic phantom. For each phantom, scans were taken centrally within the sFOV as a reference image and with the phantom edge extended at 1 cm intervals from 0 to 5 cm beyond the sFOV into the eFOV. To assess CT number accuracy various tissue equivalent materials were scanned in the eFOV and resulting CT numbers were compared to inserts scanned within the sFOV. For all phantom geometries, objects within the eFOV were geometrically overestimated with elongation of phantom shapes into the eFOV. The percentage increase in size ranged from 0.22 to 15.94 % over all phantoms considered. The difference between eFOV and sFOV CT numbers was dependent upon insert density. The eFOV underestimated CT numbers in the range of −127 to −230 HU for soft tissue densities and −278 to −640 for bone densities. This trend reversed for low tissue densities with the CT numbers in the eFOV being overestimated by 100-130 HU for lung equivalent inserts. Initial correlation between eFOV and sFOV CT numbers was seen and a correction function was successfully applied to better estimate the CT number representative of that seen within the sFOV.

Keywords

extended, field, view, image, assessment, distortion, ct, number, accuracy, within, wide, bore

Disciplines

Engineering | Science and Technology Studies

Publication Details

Beeksma, B., Truant, D., Holloway, L. & Arumugam, S. (2015). An assessment of image distortion and CT number accuracy within a wide-bore CT extended field of view. Australasian Physical and Engineering Sciences in Medicine, 38 (2), 255-261.

Australas Phys Eng Sci Med
DOI 10.1007/s13246-015-0353-6

SCIENTIFIC PAPER

An assessment of image distortion and CT number accuracy within a wide-bore CT extended field of view

B. Beeksma[1] · D. Truant[1] · L. Holloway[1,2,3,4] · S. Arumugam[1]

Received: 26 October 2014 / Accepted: 29 May 2015

Abstract Although wide bore computed tomography (CT) scanners provide increased space for patients, the scan field of view (sFOV) remains considerably smaller than the bore size. Consequently, patient anatomy which spans beyond the sFOV is truncated and the information is lost. As a solution, some manufacturers provide the capacity to reconstruct CT images from a partial dataset at an extended field of view (eFOV). To assess spatial distortion within this eFOV three phantoms were considered a $30 \times 30 \times 20$ cm^3 slab of solid water, the Gammex electron density CT phantom and a female anthropomorphic phantom. For each phantom, scans were taken centrally within the sFOV as a reference image and with the phantom edge extended at 1 cm intervals from 0 to 5 cm beyond the sFOV into the eFOV. To assess CT number accuracy various tissue equivalent materials were scanned in the eFOV and resulting CT numbers were compared to inserts scanned within the sFOV. For all phantom geometries, objects within the eFOV were geometrically overestimated with elongation of phantom shapes into the eFOV. The percentage increase in size ranged from 0.22 to 15.94 % over all phantoms considered. The difference between eFOV and sFOV CT numbers was dependent upon insert density. The eFOV underestimated CT numbers in the range of −127 to −230 HU for soft tissue densities and −278 to −640 for bone densities. This trend reversed for low tissue densities with the CT numbers in the eFOV being overestimated by 100–130 HU for lung equivalent inserts. Initial correlation between eFOV and sFOV CT numbers was seen and a correction function was successfully applied to better estimate the CT number representative of that seen within the sFOV.

Keywords Extended field of view · Computed tomography · Geometric distortion · CT number

Introduction

Computed tomography (CT) simulators are an essential component to the modern day radiation therapy treatment process. CT scanners are capable of providing three dimensional (3D) anatomical imaging, with high image resolution and good soft tissue delineation. Combined with 3D attenuation coefficient information in the form of CT numbers (Hounsfield units, HU), CT scanners have become the standard basis for radiotherapy treatment planning [1, 2]. To achieve accurate and precise radiotherapy treatment plans accurate and precise spatial and electron density information is necessary and this is usually gained from CT images. The requirements of spatial and CT number accuracy is specified by published guidelines and is recommended to be within ±1 mm and ±5 HU respectively [3].

Typically, diagnostic CT scanners have small gantry bore sizes, normally 65–70 cm diameter [2, 4] which in the radiotherapy environment, can compromise patient reproducibility and appropriateness of patient setup [2]. To

✉ B. Beeksma
bradley.beeksma@sswahs.nsw.gov.au

1 Liverpool and Macarthur Cancer Therapy Centres, Ingham Institute, Liverpool, NSW 2170, Australia

2 School of Physics, Institute of Medical Physics, University of Sydney, Sydney, NSW 2006, Australia

3 Centre for Medical Radiation Physics, University of Wollongong, Wollongong, NSW 2522, Australia

4 South Western Sydney Clinical School, University of New South Wales, Sydney, NSW 2052, Australia

Published online: 06 June 2015

address these issues, large bore CT simulators were designed specifically for the radiation therapy environment with bore sizes 80–90 cm in diameter [5] and have become commercially available by multiple manufacturers [6, 7]. The introduction of wide bore CT scanners has proved greatly beneficial within radiotherapy departments. They permit flexibility in patient set up with immobilization devices, allow greater access for interventional procedures, accommodate for bariatric patients and reduce claustrophobia.

Although these large bore CT simulators address the aforementioned physical constraints, manufacturers still only provide a conventional scan field of view (sFOV) of 50–60 cm. Under many scanning conditions portions of scanned objects can extend beyond the volume measureable by the CT detector array. This could be attributed to factors such as geometrical setup of the patient exceeding the physical beam divergence or a dimensional limitation of the detector ring. Consequently, anatomical information which may lie outside the sFOV is lost and the reconstructed image will suffer from artefacts at the site of truncation [8, 9].

Redesigning hardware components of a CT scanner to extend the sFOV would solve this problem, however this solution is not cost effective nor does it solve the problem for existing scanners. In addition to the conventional sFOV, some manufacturer's scanner models (GE LightSpeed (GE Healthcare, Wisconsin, USA), Philips Brilliance CT Big Bore (Philips Healthcare, Massachusetts, USA), Siemens Somatom Sensation Open 24 & 40 (Siemens Medical Solutions, Pennsylvania, USA), Toshiba Aquilion LB (Toshiba Medical Systems, Zoetermeer, The Netherlands) [6, 7, 10] provide the capacity to reconstruct CT images at an extended field of view (eFOV) of varying sizes. For the Philips Brilliance CT Big Bore, the reconstructed eFOV is achieved through correctional algorithms based on extrapolation of the partial data set acquired within the conventional sFOV [8, 11, 12]. The eFOV projects a representation of anatomy that lies in this boundary beyond the sFOV which may be relevant in radiotherapy treatment planning.

Reconstruction algorithms employed by most CT scanners are based on filtered back projection (FBP) or utilize iterative reconstruction methods. Depending upon the algorithm, iterative reconstruction methods can utilise FBP images to converge upon the final image [13]. FBP algorithms require that the scanned object is inside the sFOV during the entire scanning process [12]. In the eFOV region this condition is not satisfied, meaning the eFOV is generated from incomplete data. As such the HU values and distribution of the represented anatomy is not at the same level of accuracy as the true sFOV reconstructed using complete data. As a result, objects scanned within the eFOV may show significant artefacts, geometrical distortion and dissimilarity of CT number, relative to the same object scanned within the sFOV [5], such unfavourable entities are likely to induce a negative effect on the accuracy of the treatment plan.

The extent and impact of dose discrepancy due to such artefacts will vary with the particular system being considered, to date, this has been investigated to a limited extent. Wu et al. [5] used a GE LightSpeedTM RT16 CT scanner (GE Healthcare, Waukesha, WI) and showed that a SSD distortion for target delineation from geometric uncertainty can cause target dose calculation errors of 2–3 % and CT number variance can cause a 1–2 % difference in dose. Hatton et al. [14] used a cone beam CT on a Varian 2100iX linear accelerator (Varian, Palo Alto, CA) and showed that differences in CT number can influence the dose by up to 20 % in extreme cases. Kim et al. [15] did not specify the manufacturer CT imager; nevertheless they showed that imaging artefacts can result in differences in treatment plan dose distributions.

Since algorithms and their implementation will vary between systems, this study aims to evaluate the accuracy of the CT numbers and geometrical reconstruction within the eFOV for the Philips Brilliance Big Bore CT scanner.

Materials and methods

The Philips Brilliance Big Bore CT simulator is a third-generation scanner. With a physical bore size of 85 cm, it has a maximum sFOV diameter of 60 cm with the capacity to reconstruct CT images at a 70 cm eFOV. 3 kVp settings are available: 90, 120, and 140 kVp, maximum tube current of 500 mA for 90 and 120 kVp (400 mA for 140 kVp), minimum slice width of 0.6 mm with the ability to acquire a maximum of 16 slices simultaneously and a range of CT number display of −1024 to +3072 HU.

Accuracy of spatial data in eFOV region

To assess spatial distortion, three phantom geometries were considered; a $30 \times 30 \times 20\ cm^3$ slab of Solid Water (Gammex Inc, Middleton, Wisconsin, USA), the 33 cm diameter Gammex Electron Density CT phantom (Gammex Inc, Middleton, Wisconsin, USA) and a female anthropomorphic phantom (CIRS, Norfolk, Virginia, USA). These are shown in Fig. 1.

At its widest point the anthropomorphic phantom has a diameter of 35 cm. The widest edge of each of the phantoms was used as the reference point for purposes of positioning the phantom. For each phantom, scans were taken at five positions within the eFOV and one position centrally within the sFOV. For each scan within the eFOV, the phantom edge was shifted laterally at 1 cm intervals

Fig. 1 Phantoms used for assessment of spatial distortion. From *left* to *right* solid water, CT electron density phantom and anthropomorphic phantom

from 0 to 5 cm beyond the sFOV into the eFOV (see Fig. 2). These 1 cm lateral offsets ensured that the phantom was imaged over the full range of the eFOV region. For all scans and phantom geometries an identical full helical standard pelvis protocol was used with the following settings, 120 kV, 250 mAs, 70 cm FOV, 0.688 pitch, 16 × 1.5 collimation and 2 mm slice thickness. Data was reconstructed using a filtered back projection based reconstruction algorithms.

Acquired images were imported into Pinnacle[3] (Version 9.0, Philips Healthcare, USA), for quantification of image distortion. For each of the three phantoms, a standard contour was generated based on the reference image. The area of the reference contour was calculated based on the mean value of 3 consecutive slices using Pinnacle's volume measuring tool. This contour was then copied onto each of the images scanned within the eFOV as a representation of the phantoms physical geometry (Fig. 3a, b). For each of the lateral offset positions within the eFOV, the geometry of each phantom was contoured (Fig. 3c) at the slice where maximum geometric distortion was observed. The area of the contour was then computed using Pinnacle's volume measuring tool. Based on a single slice, the difference in area between the contour from the eFOV and from the standard was quantified as the distortion (Fig. 3d).

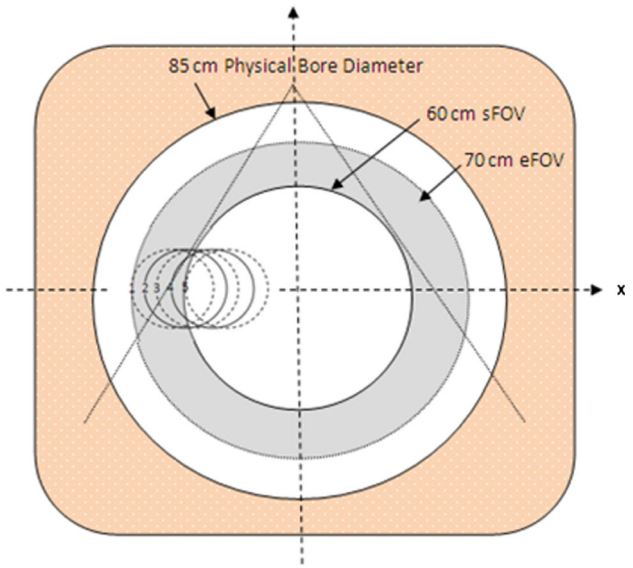

Fig. 2 Schematic illustration of the lateral offset used to assess geometrical distortion. A 1 cm displacement is applied between subsequent phantom positions from the scan field of view (sFOV) into the extended field of view (eFOV)

eFOV CT number

To assess the accuracy of CT numbers within the eFOV, the CT number of various compositions of tissue equivalent inserts imaged in the eFOV was compared to the CT number of the same inserts scanned centrally within the sFOV using an identical scan protocol. The tissue equivalent inserts scanned were LN-300 Lung, LN-450 Lung, Adipose, Breast, Solid water, True water, Brain, Liver, Inner bone, B-200 bone, CB2—30 %, CB2—50 % and Cortical bone with relative electron densities of 0.26, 0.41, 0.93, 0.96, 0.99, 1.00, 1.05, 1.07, 1.10, 1.11, 1.27, 1.47 and 1.70 respectively.

To avoid potential inconsistencies in reproducing identical setup positions, the Gammex Electron Density CT phantom was positioned with its edge 35 cm from central axis. This correlates to a 5 cm offset from the sFOV into the eFOV and permitted the 3 cm diameter tissue insert holder to be positioned entirely within the eFOV. This allowed the tissue insert to be easily interchanged between scans whilst ensuring reproducibility of tissue insert location. The CT protocol used was a full helical standard pelvis protocol with 120 kV, 250 mAs, 70 cm FOV, 0.688

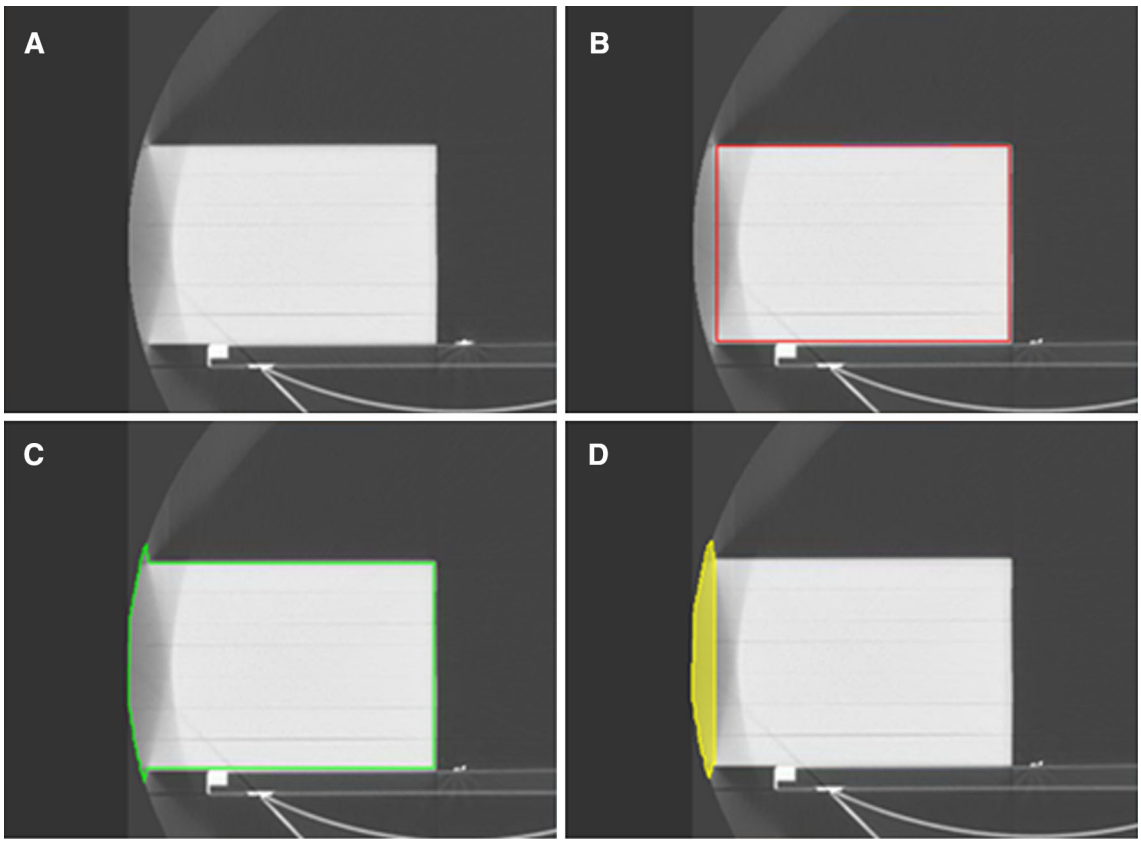

Fig. 3 Methodology of contouring used for quantification of image distortion. **a** Solid water imaged at 120 kV, 250 mAs and a 3 cm offset from the edge of the sFOV **b** Reference image contour (*red*) based on scan centrally within the sFOV **c** Object contoured including geometrical distortion (*green*) **d** Subtraction of **b** from **c** indicating geometric distortion

pitch, 16 × 1.5 collimation and 2 mm slice thickness. For each tissue insert, a 15 mm diameter circular region of interest (ROI) tool was used to calculate the mean CT number of each insert. The ROI was placed centrally over the insert ensuring the ROI did not intersect the boundary of the insert with the Gammex phantom. The ROI was drawn consistently over three consecutive slices the mean CT number was recorded. The uncertainty associated with this reading was based on a single standard deviation of the CT number within the ROI. Error in the eFOV CT number was evaluated by comparison to a baseline CT number which was defined by taking an identical scan of the phantom and the insert located centrally within the sFOV.

Results and discussion

Accuracy of spatial data in eFOV region

As depicted in Fig. 4, the eFOV reconstruction algorithm induces severe image artefacts in the lateral direction within the region outside the 60 cm sFOV. Although still apparent, a lesser extent of distortion was seen in the anterior/posterior direction. This is attributed to the positional location of the phantom. Placement of the phantom at the anterior border of the CT field of view, would result in greater distortion in the anterior/posterior direction and lesser in the lateral. For all phantom geometries, objects displaced within the eFOV were geometrically overestimated with elongation and bludging of each of the phantom edges into the eFOV. The size of the object was not reduced in the eFOV for any of the considered situations. The elongation is seen to be truncated at the 70 cm field of view, resulting in a sharp curved phantom edge and thus an inaccurate indication of the geometrical shape of the phantom. The eFOV algorithm does not extrapolate information beyond the 70 cm field of view. The distortion of the geometry of the phantom can be easily seen by comparing the reference scan of the centrally scanned phantom to the same phantom with various applied offsets. Based on the slice which displayed the greatest distortion, Table 1 gives a quantitative analysis of the area over estimation for phantoms placed at different intervals within the eFOV. Depending upon the size of the displacement, the size of the area overestimation ranged from 0.22 to 15.94 % for all phantom geometries considered. The

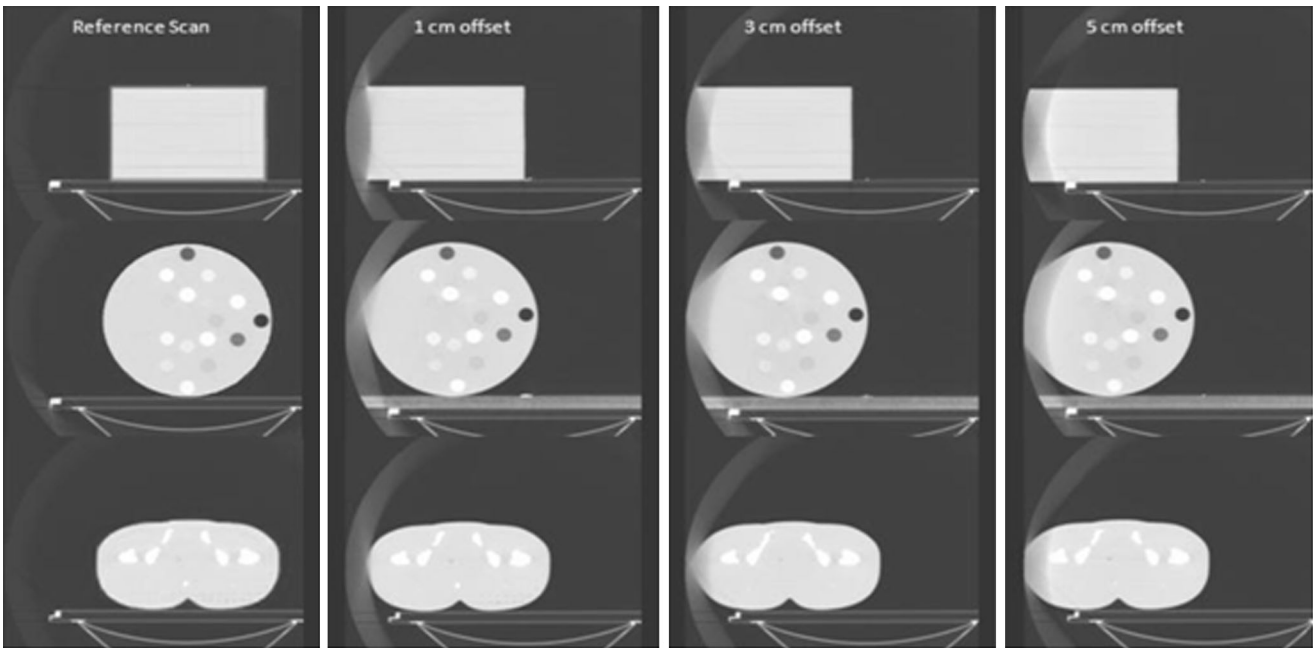

Fig. 4 Image distortion for the three phantom geometries displaced at different intervals within the eFOV

Table 1 Quantification of distortion for phantoms displaced 1–5 cm beyond the sFOV

Offset (cm)	Percentage increase in area per 2 mm slice		
	Circular phantom	Square phantom	Anthropomorphic
1	0.73	15.94	0.22
2	1.29	10.48	0.91
3	2.24	6.29	1.05
4	1.56	2.94	1.49
5	0.43	0.39	0.85

square and circular phantoms obviously do not reflect typical anatomical shapes seen in patients. However, these phantoms do indicate that the extent of distortion is dependent upon anatomical shape within this region, thus the magnitude of spatial distortion will vary with individual patient anatomy within the scanned region. Table 1 depicts the percentage increase in area relative to the true phantom area. Since the reconstruction truncates to a maximum FOV of 70 cm, with greater phantom displacement into the eFOV, a greater volume of 'real phantom' is therefore placed within the eFOV and consequently must be subtracted from the contour in order to gauge the area of distortion. For this reason the quantification of distortion is different for each phantom at each offset and for the square and circular phantom the percentage area appears to decrease with increased offset.

When the phantom was entirely contained to the sFOV no artefact or geometrical distortion were seen on the image; all images showed some degree of artefact and distortion when phantoms were scanned in the eFOV. Such artefacts are evident where the phantom insects the border of the sFOV. In all images, a brightening artefact can be seen at the sFOV boundary. This is an indication of an over estimation of CT number at this location. This issue has been investigated in the literature.

Li et al. [8] was able to improve image quality and suppress boundary artefacts seen at the eFOV/sFOV interface. Additionally, CT number uniformity is claimed to be improved with the application of their algorithm, however no statement is made which references the accuracy of the CT number itself relative to the sFOV and how accurate the algorithm calculates CT numbers for materials of different densities. Ohnesorge et al. [9] describes an algorithm which is able to correct boundary image artefacts caused by objects outside the sFOV. Within these artefact corrected regions, the accuracy of the CT number is stated to be vastly improved to a number representative of that seen centrally within the sFOV, however, no reference is made to the objects spanning outside the sFOV. Wu et al. [5] describes the use of the heterogeneity correction

algorithm on dose computation accuracy using the Eclipse treatment planning system. <1 % error in dose calculation error is stated for volumetric modulated arc therapy plans. However, this algorithm is independent of the acquired image and does not correct for geometrical distortion nor CT number accuracy of the image. The authors suggest that variance in contour distortion and CT numbers have effectively cancelled each other out. The application of such algorithms to images acquired with the Philips Brilliance Big Bore CT scanner has the potential to improve HU number accuracy and minimise the image artefacts seen at eFOV/sFOV, however deliberation of the aforementioned limitations should be considered. Alternately, the use of iterative reconstruction methods has been shown to be feasible to enhance image quality compared to FBP algorithms [16–18]. Although not assessed in this study the application of different iterative reconstruction algorithms may provide enhanced imaging accuracy within the eFOV region.

eFOV CT number

Figure 5 illustrates the accuracy of CT numbers generated within the eFOV by comparison to baseline CT numbers generated within the sFOV. CT numbers generated in the eFOV, for tissue inserts of densities greater than lung, showed a trend of being under estimated compared to identical scans of the inserts conducted centrally within the sFOV. The disparity between eFOV and sFOV CT number worsened with increasing tissue density with the difference in eFOV and sFOV CT number variation ranging from −103 to −132 HU for soft tissue densities and −190 to −488 for bone densities. This trend reversed for low tissue densities with the CT numbers in the eFOV being overestimated by 100–130 HU for lung equivalent inserts. These results reflect a similar trend in estimation of CT numbers within the eFOV previously stated by Wu et al. [5] using the GE lightspeed CT scanner. These values fall far beyond the acceptable published guidelines [3] of ±5 HU CT number accuracy requirements for CT scanners in the radiotherapy environment. The standard deviation of the CT number within the ROI was seen to be much greater for those produced within the eFOV compared to the sFOV. This trend is expected; as the reconstruction algorithm is calculating CT numbers based on an incomplete dataset. The greater the CT number, the worse the algorithm will estimate the true HU value.

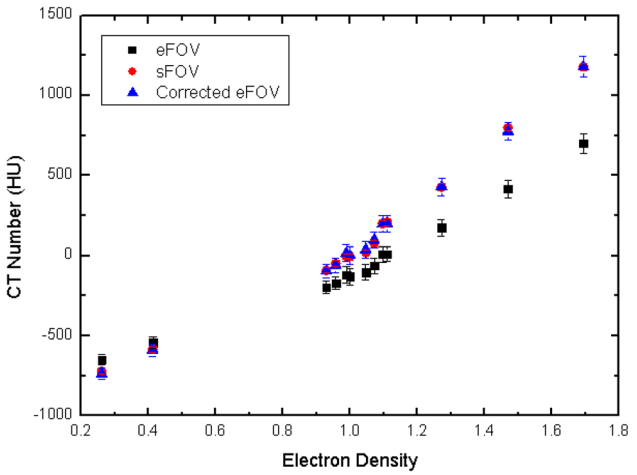

Fig. 5 Comparison of CT numbers generated within the eFOV, centrally within the sFOV and those within the eFOV corrected using a predictive correlation function

The disparity of CT numbers calculated in the eFOV and the sFOV was investigated. A strong correlation between HU in the eFOV and its respective HU in the sFOV was seen. Based on this relationship, a predictive correction function was derived and applied to the eFOV CT numbers to better represent that of the true CT number indicated in the sFOV. As shown in Fig. 5, initial correlation shows that, within error, the function was successfully able to estimate a CT number representative of that seen within the sFOV. The error in the corrected eFOV number was acquired by adding the error of the eFOV and sFOV in quadrature. The greatest disparity between the corrected and sFOV CT number was found to be 22 HU for the CB2—50 % bone insert. The application of such a function to CT numbers within the eFOV could drastically reduce error in CT number within this region; however assessment of the accuracy across different CT scanners, protocol and function of position still needs to be assessed. Although the predictive function has vastly reduced the difference between the number seen within the eFOV and sFOV, the shown discrepancy still falls outside the AAPM TG66 [3] recommendations of CT number accuracy of ±5 HU. Additionally, this function provides no improvement to distortion of the contour and the user must be aware that spatial inaccuracies are still apparent.

Radiotherapy treatment planning systems rely on CT numbers to correct for patient tissue inhomogeneity. Inaccuracies in CT number calculation will therefore carry through into inaccuracies in dose computation. Clinically, patient extremities are the most probable tissues to be present within the eFOV, however, within the radiotherapy environment immobilisation devices and set-up equipment may encroach the region. Such devices are often composed of materials such as plastic or carbon which typically have CT numbers close to that of water. Consequently CT numbers within the eFOV are more probable to be representative of water than that of high or low density materials.

The impact of both the inaccuracy of spatial accuracy and CT numbers within the eFOV on a radiotherapy

treatment plan is beyond the scope of the current study. The impact on the resulting radiation dosimetry would depend on the anatomy being considered and the radiotherapy treatment technique. However, it is evident from this work that the magnitude of error seen within the eFOV is large enough to warrant further dosimetric study.

Conclusion

The eFOV feature provides a general visual representation of the geometry which exists outside the sFOV; however, significant image artefacts from the eFOV reconstruction alter the CT numbers and geometric contours of shapes within this region. The physical edge of any phantom considered in this study was unable to be reproduced within the eFOV without severe geometrical distortion. The percentage increase in size ranged from 0.22 to 15.94 % for all phantom geometries considered. For the same tissue inserts, CT numbers generated within the eFOV show a vast disparity to those generated in the sFOV. The difference in CT number between the sFOV and eFOV range from −190 to −488 for bone densities, −103 to −132 HU for soft tissue densities and 100–130 HU for lung equivalent densities. The extent of variation appeared to be dependent upon the density of the material. CT numbers for high density objects were underestimated with a greater discrepancy being seen with increasing density. The contrary was seen for low tissue density materials with the CT number being overestimated. A correlation between CT numbers in the eFOV and sFOV was found. A correction function was able to be applied to CT numbers in the eFOV to closer predict the expected value. Although tissues of excessively high or low density (such as bone or lung) are rarely seen at the extremity of patient contours, it is recommended that vigilant revision of patient anatomy within the eFOV region should be undertaken prior to the clinical use of the eFOV reconstruction.

References

1. McGee K, Das I, Sims C (1995) Evaluation of digitally reconstructed radiographs (DRRs) used for clinical radiotherapy: a phantom study. Med Phys 22:1815–1827
2. Garcia-Ramirez J, Mutic S, Dempsey J, Low D, Purdy J (2002) Performance evaluation of an 85-cm-bore x-ray computed tomography scanner designed for radiation oncology and comparison with current diagnostic CT scanners. Int J Radiat Oncol Biol Phys 52:1123–1131
3. Sasa M, Palta J, Butker E, Das I, Huq MS, Loo LN, Salter BJ, McCollough CH, Van Dyk J (2003) Quality assurance for computed-tomography simulators and the computed tomography-simulation process: report of the AAPM radiation therapy committee task group no. 66. Med Phys 30(10):2762–2792
4. Zhang J, Sehgal V, He B, Roa D, Martin M, Al-Ghazi M (2010) Comprehensive clinical commissioning and quality assurance procedures of a big bore CT simulator in a radiation oncology department. Med Phys 37:3152
5. Wu V, Podgorsak M, Tran T, Malhotra H, Wang I (2011) Dosimetric impact of image artifact from a wide-bore CT scanner in radiotherapy treatment planning. Med Phys 38(7):4451–4463
6. Centre for Evidence-Based Purchasing (2009) Comparative specifications: wide bore CT scanners. Report no. CEP 08029. NHS Purchasing and Supply Agency, London
7. Centre for Evidence-Based Purchasing (2006) Wide bore CT scanner comparison: report 06014. NHS Purchasing and Supply Agency, London
8. Li B, Deng J, Lonn A, Hsieh J (2012) An enhanced reconstruction algorithm to extend CT scan field-of-view with z-axis consistency constraint. Med Phys 39(10):6028–6034
9. Ohnesorge B, Flohr T, Schwarz K (2000) Efficient correction for CT image artifacts caused by objects extending outside the scan field of view. Med Phys 27(1):39–46
10. Centre for Evidence-Based Purchasing (2005) GE LightSpeed RT CT scanner technical evaluation. NHS Purchasing and Supply Agency, London
11. Zamyatin A, Nakanishi S (2007) Extension of the reconstruction field of view and truncation correction using sinogram decomposition. Med Phys 34(5):1593–1604
12. Hsieh J, Chao E, Thibault J, Grekowicz B, Horst A, McOlash S, Myers T (2004) A novel reconstruction algorithm to extend the CT scan field-of-view. Med Phys 31(9):2385–2391
13. Beister M, Kolditz D, Kalender W (2012) Iterative reconstruction methods in X-ray CT. Phys Med 28:94–108
14. Hatton J, McCurdy B, Greer P (2009) Cone beam computerized tomography: the effect of calibration of the Hounsfield unit number to electron density on dose calculation accuracy for adaptive radiation therapy. Phys Med Biol 54:329–346
15. Kim Y, Tome W, Bal M, McNutt T, Spies L (2006) The impact of dental metal artifacts on head and neck IMRT dose distributions. Radiother Oncol 79:198–202
16. Korn A, Fenchel M, Bender B, Danz S, Hauser TK, Ketelsen D, Flohr T, Claussen CD, Heuschmid M, Ernemann U, Brodoefel H (2012) Iterative reconstruction in head CT: image quality of routine and low-dose protocols in comparison with standard filtered back-projection. AJNR Am J Neuroradiol 33(2):218–224
17. Mitsumori L, Shuman W, Busey J, Kolokythas O, Koprowicz K (2012) Adaptive statistical iterative reconstruction versus filtered back projection in the same patient: 64 channel liver CT image quality and patient radiation dose. Eur Radiol 1(22):138–143
18. Nuyts J, DeMan B, Dupont P, Defrise M, Suetens P, Mortelmans L (1998) Iterative reconstruction for helical CT: a simulation study. Phys Med Biol 43(4):729–737